A Dual-Slot Barrier Sensor for Partial Discharge Detection in Gas-Insulated Equipment

Christos Zachariades, Roger Shuttleworth, Riccardo Giussani, *Member, IEEE*

***Abstract*— This paper reports on the development and testing of a novel barrier sensor for UHF Partial Discharge (PD) detection in gas-insulated equipment. The sensor features a unique dual-slot planar antenna backed by an air-filled cavity. The dual-slot arrangement allows different parts of the antenna to resonate at different frequency ranges in the UHF spectrum. As a result, the sensor exhibits broader bandwidth and higher sensitivity than other barrier sensors. Finite Element Analysis simulations have been used to optimize the sensor design. Furthermore, testing using a specially made PD test rig, GTEM cell testing and testing on a gas-insulated line section in the high voltage laboratory, have validated the simulation results and the capabilities of the sensor. The Dual-Slot Barrier (DSB) sensor exhibits a bandwidth of 0.3 - 2.0 GHz with a mean effective height of 13 mm, and an effective height above 2 mm for 90% of the frequency range. The sensor can be used with both wideband instruments, such as oscilloscopes, and narrow band instruments such as frequency downconverters. Additionally, its optimized dimensions and unique replaceable sealing attachment ensure maximum compatibility for retrofitting on a wide range of equipment.**

***Index Terms*— bowtie antenna, condition monitoring, finite element analysis (FEA), gas-insulated switchgear (GIS), partial discharge (PD), sensor, slot antenna, UHF couplers.**

I. Introduction

Partial Discharges (PDs) can provide information regarding the condition of High Voltage (HV) insulation and their monitoring can be used to detect incipient faults and inform the performance of maintenance operations to prevent equipment failure. In gas-insulated equipment common causes of PD include metallic particles, protrusions on the HV conductor and defects in insulating supports.

Due to the nature of the equipment, which must be sealed to prevent the insulating medium from escaping to the environment, the use of capacitive or inductive PD sensors [1], and PD measurements according to IEC 60270 [2] are not feasible in most cases. To facilitate PD detection in such equipment Ultra-High Frequency (UHF) sensors are often employed [3]. Several types of UHF sensors are available, including UHF probes used for power transformers [4] as well as standard-type and non-conventional sensors used for gas-insulated switchgear (GIS) [5]. Because external noise does not significantly affect the detection capabilities of UHF sensors, the UHF method can have a sensitivity comparable to more traditional PD detection techniques [2].

However, employing UHF methods for PD detection is not without challenges. Not all GIS equipment comes with sensors installed from the factory. Retrofitting internal sensors can be problematic since the equipment must be de-energized and the insulating medium emptied. Furthermore, existing UHF sensors may be repurposed from other applications and not originally designed for PD detection. Lack of critical characteristics such as wideband response and high sensitivity to low-amplitude, impulsive signals can lead to failed detection or misclassification of defects [6].

To allow for PD monitoring of equipment where internal sensors are not installed, external sensors can be placed on top or very close to an exposed area of an insulating barrier or support. The sensors must have wideband frequency characteristics since the PD signals are pulsed and contain multiple frequencies. As mentioned earlier, PD can be generated by different types of defects resulting in signals of different frequencies. Additionally, the geometry of the plant and PD pulse propagation distance from its source to the sensor can also affect the detectable frequencies. However, the geometry of the insulating barrier can severely constrain the dimensions of external sensors and directly conflict with the requirement for wideband response.

This paper describes the development, testing and deployment of a Dual-Slot Barrier (DSB) sensor which can be retrofitted onto HV gas-insulated equipment to enable the use of the UHF method for PD detection. The wideband response of the sensor in the UHF spectrum has been achieved by designing a novel dual-slot planar antenna backed by a cavity. The performance of the sensor was fine-tuned using finite element simulations to optimize its dimensions. Additionally, a simulation methodology has been implemented to successfully estimate the effective height (inverse antenna factor) parameter, which is often used as a measure of UHF PD sensor performance. The capabilities of the sensor have been extensively tested in the laboratory and its performance has been compared against other commercially available barrier sensors during side-by-side testing. Moreover, DSB sensors have been retrofitted on a Gas-Insulated Line (GIL) section where PD tests were performed alongside internal UHF sensors.

II. Sensor Design

UHF barrier sensors are normally installed on the outside of HV equipment, on top or very close to an exposed area of an insulating barrier or support. For GIS these are the barrier insulators that separate different compartments. Although the

Manuscript received July 09, 2019; revised September 20, 2019; accepted September 20, 2019. This work was co-funded by the UK's Innovation Agency, Innovate UK. Paper no. .

C. Zachariades is with the University of Liverpool (e-mail: C.Zachariades@liverpool.ac.uk), Liverpool, M13 9PL, UK.

R. Shuttleworth is with the University of Manchester (e-mail: roger.shuttleworth@manchester.ac.uk), Manchester, M13 9PL, UK.

R. Giussani is with High Voltage Partial Discharge Ltd (e-mail: riccardo.giussani@hvpd.co.uk), Salford, M50 2UW, UK.

Color versions of one or more of the figures in this paper are available online at http://ieeexplore.ieee.org. Digital Object Identifier .

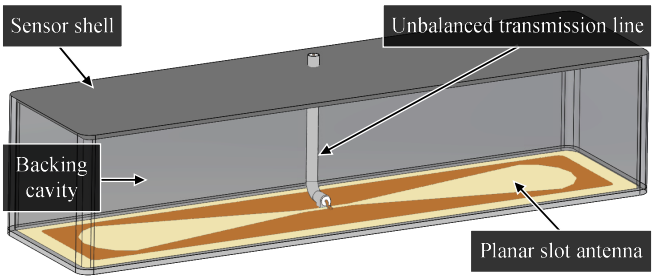

Fig. 1. DSB sensor concept. The sensors consists of a planar slot antenna backed by a cavity and fed by an unbalanced transmission line.

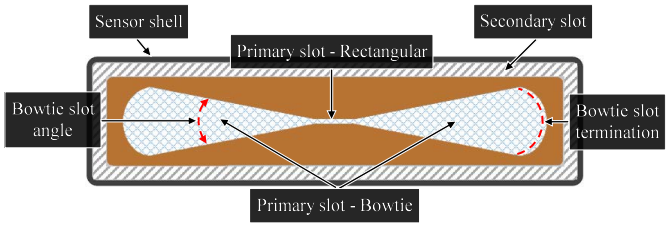

Fig. 2. DSB sensor planar antenna. The inner slot consist of two triangular sections (bowtie) joined by a rectangular section in the middle. The outer slot is formed between the metallization of the PCB and the shell of the sensor.

outer rim of the barrier insulator can be completely exposed, in many applications it is covered with a metallic band. The band is either present because of the casting manufacturing process for the insulator or is added after installation to provide additional mechanical protection and ensure ground continuity for the various interconnected sections. Hence, the dimensions of the barrier sensor are severely constrained by the geometry of the insulating barrier and the available exposed area on the insulator, often referred to as casting aperture. These constraints directly conflict with the requirement for wideband response, which is vital for reliable condition diagnosis.

With the above in mind, the DSB sensor design was conceived, with the aim to develop a novel sensor which exhibits wideband frequency response and high sensitivity in the UHF spectrum, while maintaining the restricted dimensions imposed by the geometry of insulating barriers. The sensor comprises a planar antenna backed by a cavity and fed by a short unbalanced transmission line (Fig. 1). The length and width of the antenna were constrained to 190 mm and 60 mm respectively from the beginning of the development process, since it was determined that these dimensions would give the sensor maximum compatibility with a wide variety of HV assets.

The sensor design is based on the cavity-backed slot antenna [7, 8]. However, it differs substantially from the majority of such antennas since it offers several unique features introduced to allow for optimal PD detection performance. The main elements of the sensor are the following:

- A shell comprised of electrically conducting material forms a backing cavity.
- A printed circuit board (PCB), forms a planar antenna. The PCB is positioned at the opening of the shell but the PCB copper layer does not make contact with the shell.
- The centre part of the PCB copper layer is etched to form a rectangular middle slot section flanked by triangular slot sections extending from the ends of the rectangular slot section, which in turn are terminated with circular segments. They form the primary slot of the antenna (Fig. 2).
- The gap between the PCB conducting layer and the shell of the sensor forms a secondary antenna slot.
- An unbalanced transmission line feeds the antenna, and allows connection to a signal cable via a coaxial connector.

The outer secondary slot of the antenna fully encircles the inner primary slot. This unique dual-slot configuration allows the antenna to exhibit multiple resonance modes over a wide frequency range. The secondary slot enables detection of signals at the lower end of the antenna's frequency range while the primary slot enables detection at the intermediate and higher end of the frequency range. The shape and dimensions of the slots as well as the dimensions of the cavity in relation to the dielectric surface of the antenna ensure adequate impedance matching and efficiency over a wide frequency range. The cavity also provides electrical shielding to the antenna and improves the front-to-back ratio [7].

The signal feeding method utilized was designed with the unique characteristics of the sensor in mind. While a microstrip transmission line [9, 10] and a coplanar waveguide [11, 12] were considered, they were found to cause issues, in practice, with the installation of the sensor. Hence, the feed for the DSB sensor antenna was designed as an unbalanced transmission line constructed from RG223 coaxial cable (Fig. 1). The cable connects across the rectangular section of the primary slot. In, addition, the shield wire is electrically connected to the sensor shell. This feeding method ensures that the characteristic impedance of the sensor at the signal cable attachment point is 50 Ω, and allows the sensor to interface directly with many monitoring instruments.

III. Optimization by Simulation

To optimize the DSB sensor performance, Finite Element simulations were employed. Various geometric characteristics of the sensor were parametrized and transferred from a Computer Aided Design (CAD) software package into COMSOL Multiphysics. Computations were performed in the range 0.2 – 2.7 GHz in 0.1 GHz steps. The main aim of the optimization process was to achieve a reflection coefficient (S11 parameter) lower than – 6 dB in the 1.0 – 2.0 GHz range. This range was selected for a variety of reasons. Previous studies have found an upper limit of 2 GHz to be of practical significance for UHF PD detection in GIS [13, 14]. On the other hand, interference from corona discharges, which can be prevalent in HV substations and can increase the noise level, tends to diminish above 0.5 GHz [3]. A reflection coefficient of S11 = -6 dB (25% reflected power) was considered a reasonable compromise between performance and cost given the restricted dimensions of the sensor. Furthermore, the sensor is intended to be used only as a detector, hence there would be no risk of reflected power damaging the instrumentation. It is important to note that the reflection coefficient was not used to determine the bandwidth of the sensor. A different measure of bandwidth was used which is described in detail in Section V. In the following sections, optimization of the three most

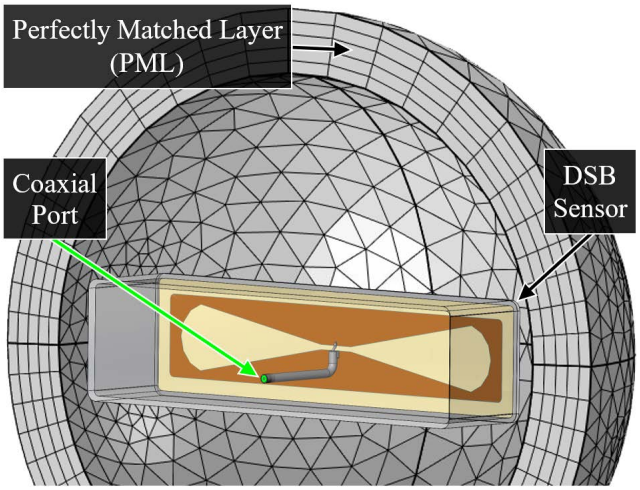

Fig. 3. Discretized computation domain surrounding the DSB sensor model. The outer PML domain absorbs all outgoing wave energy without impedance mismatch while the model is excited by a 50 Ω coaxial lumped port.

influential features is detailed, specifically the dimensions of the two slots and the cavity. These have been optimized one at a time using an iterative approach. Additionally, other properties have also undergone optimization, such as the shape and position of the feed structure, the distances between the primary and secondary slots, and the materials used for the sensor construction.

A. Simulation Setup

For optimization of sensor parameters, the COMSOL Multiphysics RF Module was utilized. Using the Finite Element Method (FEM), the module formulates and solves the differential form of Maxwell's equations accounting for initial and boundary conditions. The time-harmonic wave equation for the electric field (1) is solved which is available through the *Electromagnetic Waves, Frequency Domain* interface.

$$\nabla \times \left(\mu_r^{-1} \nabla \times \mathbf{E} \right) - k_0^2 \varepsilon_r \mathbf{E} = 0 \tag{1}$$

$\mathbf{E}$ is electric field, ε_r is the relative permittivity, μ_r is the relative permeability and k_0 is the wave number of free space.

The *Perfect Electric Conductor (PEC)* boundary condition was used to model the metallic surfaces including the shell of the sensor, the conductor and shield of the transmission line and metallization on the PCB. This boundary condition simplifies the computation by setting the tangential component of the electric field to zero (2), hence the metallic parts are considered to be lossless for the purposes of the simulation.

$$\hat{\mathbf{n}} \times \mathbf{E} = 0 \tag{2}$$

To specify the location at which energy enters and exits the model, the *Lumped Port (Coaxial)* boundary condition was used to facilitate the excitation of the model. The port was defined as being on the edge of the transmission line exiting the sensor shell, which would normally correspond to the location of the connector for the signal cable. With this boundary condition assigned the transmission line was set to operate in the Transverse Electro-Magnetic (TEM) mode. The characteristic impedance of the port was set to match that of the connector i.e. 50 Ω.

TABLE I
MATERIAL PROPERTIES FOR COMPUTATION

Component	Material	Conductivity (S/m)	Relative permittivity	Relative permeability
PCB substrate	FR4	0.004	4.5	1.0
Balun insulation	Polyethylene	0	2.3	1.0
Enclosing domain	Air	0	1.0	1.0

TABLE II
MESH PARAMETERS

Frequency step (GHz)	Number of elements	Minimum element size (mm)	Maximum element size (mm)	Minimum element quality
0.3	430 535	0.037	200	0.037
1.5	430 997	0.037	40	0.030
2.7	440 921	0.037	22	0.037

A spherical domain surrounded by a Perfectly Matched Layer (PML) [15] was used to encapsulate the sensor model in COMSOL (Fig. 3). The PML stretches the simulation domain so that the simulation can be performed as if the sensor is suspended in free space, avoiding reflection of energy from the outer boundary. '*Polynomial*' stretching, defined in equation (3), was preferred since the simulations are concerned with electromagnetic waves of a single wavelength.

$$f_p(\xi) = s\xi^p(1-i) \tag{3}$$

f_p is the stretching function, ξ is a dimensionless parameter that can vary between 0 and 1, p is the curvature parameter, s is the scaling factor, i is the unit imaginary number.

The computation takes into account the insulating material properties, which are inputs to the constituent relationship of equation (1) i.e. the electrical conductivity, relative permittivity and relative permeability. Table I presents the values used for the sensor components. The properties of the materials change insignificantly with frequency in the range of interest hence they have been considered to be constant for the purposes of the simulation.

Discretization of the mesh for the geometry was performed automatically by COMSOL using the *physics-controlled mesh* option. With this option selected the mesh size is parameterized based on frequency i.e. the mesh size, and consequently the number of elements, is adjusted automatically when the frequency changes. As a result the memory requirements and the computation time for the simulation are minimized since the optimal size of elements is selected for each frequency step. Regardless, appropriate checks were made to ensure the quality of the mesh. It was ensured that at least five second-order Lagrangian elements were used per wavelength [16-18]. Furthermore, at least two second-order elements were used per 90° arc [19] and the minimum element quality was always maintained above 0.01. The main mesh parameters for three frequency steps representative of the range of the simulation are shown in Table II.

B. Optimization of the Primary Slot

The primary slot of the DSB sensor antenna is a combination of a rectangular slot and a bowtie slot with semi-circular

This article has been accepted for publication in a future issue of this journal, but has not been fully edited. Content may change prior to final publication. Citation information: DOI 10.1109/JSEN.2019.2943625, IEEE Sensors Journal

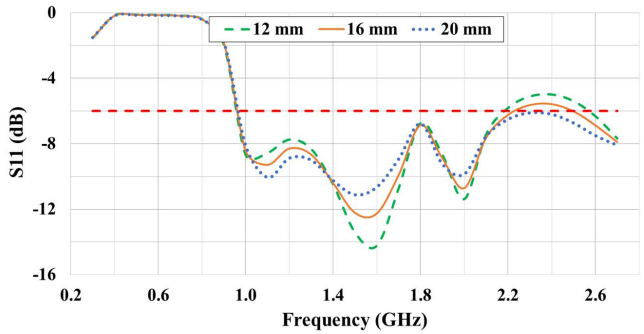

Fig. 4. Effect of the rectangular slot length to the reflection coefficient of the DSB sensor.

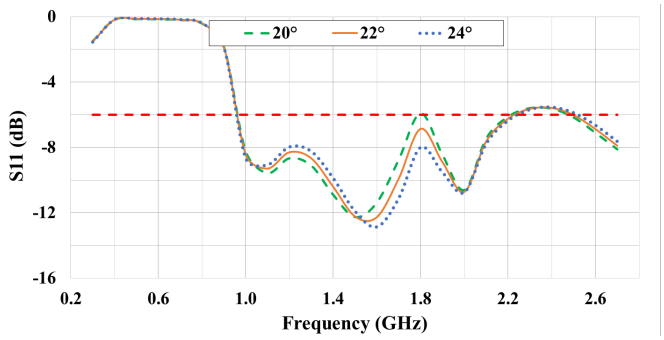

Fig. 5. Effect of the bowtie slot angle to the reflection coefficient of the DSB sensor.

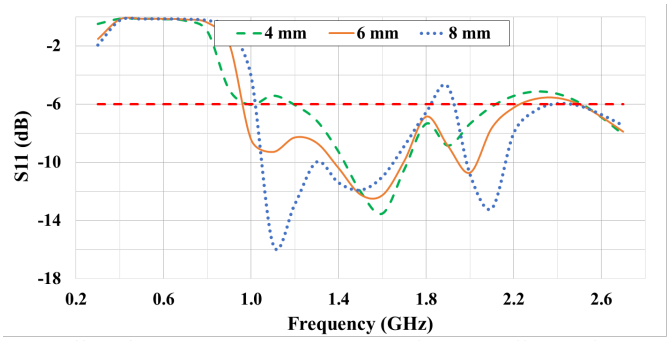

Fig. 6. Effect of the secondary slot width to the reflection coefficient of the DSB sensor.

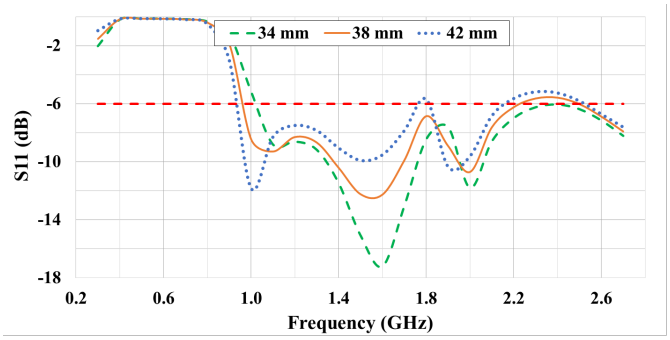

Fig. 7. Effect of the cavity height to the reflection coefficient of the DSB sensor.

terminations. Examining the centrally located rectangular section first, it was observed that increasing its length significantly affected two areas of the frequency response plot, the first between 1.4 and 1.7 GHz, and the second above 2.2 GHz (Fig. 4). An increase in length resulted in a flatter response curve which is a desirable characteristic for the sensor.

The effect of the angle of the bowtie slot section is shown in Fig. 5. Increasing the angle (Fig. 2) increased the reflection coefficient in the 1.5 – 1.9 GHz range but at the same time decreased it slightly between 1.1 – 1.4 GHz. Also, increasing the radius of the convex bowtie termination sections had a similar but less pronounced effect in the same frequency ranges.

C. *Optimization of the Secondary Slot*

One of the unique features of the DSB sensor is the incorporation of the antenna secondary slot. It is formed by leaving a non-metalized area at the edge of the board. The secondary slot is consequently formed between the copper layer which defines the primary slot and the shell of the sensor.

The effect of the width of the secondary slot on the frequency response of the sensor is substantial and can be seen in Fig. 6. Slot widths of 4 mm and 8 mm show strong resonances at specific frequencies. Additionally, they restrict the bandwidth of the sensor at both ends of the spectrum. It is evident that the optimum width is 6 mm. This provides the widest bandwidth and the flattest response with a reflection coefficient consistently below -6 dB between 1.0 and 2.2 GHz.

D. *Optimization of the Cavity*

Another highly influential geometric parameter of the DSB sensor was the size of the cavity behind the planar antenna. Typically, increasing the volume of the cavity increases the bandwidth. In this case, the only dimension that could be varied was the height of the cavity since the length and width were constrained to ensure compatibility with barrier insulators. The effect on the frequency response is shown in Fig. 7. The smoothest response curve with a reflection coefficient below – 6 dB between 1.0 and 2.2 GHz is achieved with a height of 38 mm.

Another aspect of the cavity that is subject to optimization is the dielectric medium with which it can be filled. Simulations performed using dielectrics with higher permittivity than air confirmed what is reported in the literature in relation to cavity backed antennas [20]. The resonant length of the slot becomes effectively smaller, which in turn can allow the dimensions of the antenna to be reduced. At the same time however, it adversely affects the bandwidth and efficiency. As a result, the best option for the barrier sensor is to leave the cavity filled with air.

IV. Sensor Construction

After a proof-of-concept prototype, based on the outcome of the optimization process, was used to verify the functionality of the concept, a functional prototype of the barrier sensor was constructed as shown in Fig. 8. Since the sensor is to be installed indoors as well as outdoors it was designed to be dust and water resistant, rated IP68 according to EN60529 [21].

To facilitate the connection to a low-loss coaxial cable, the antenna feed was connected internally to a Threaded Neill-Concelman (TNC) connector with the connector ground being electrically connected to the shell of the sensor. This type of connector serves multiple purposes. Firstly, it ensures appropriate operation of the sensor in the UHF spectrum since it is rated for frequencies up to 11 GHz and it also has a 50 Ω impedance. Secondly, it minimizes the chances of connecting

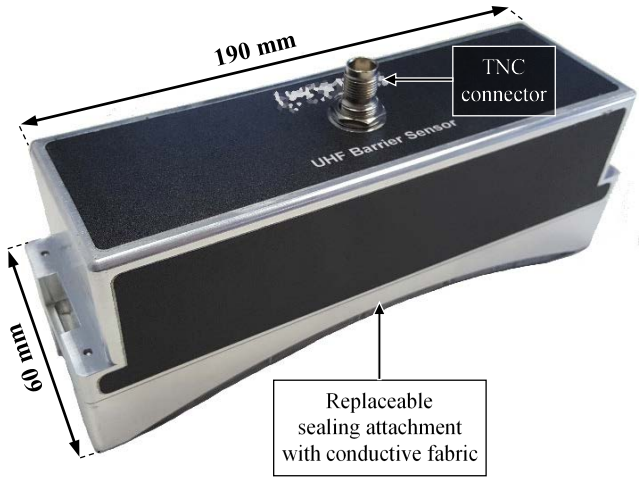

Fig. 8. UHF Barrier sensor, showing main components and dimensions. The replaceable sealing attachment allows the sensor to be installed on HV equipment of different sizes.

the sensor to lower bandwidth, BNC-terminated coaxial cables used for other PD sensors which would degrade the signal quality. Finally, a rubber gasket ensures a watertight seal with the sensor shell once the cable is connected.

In addition to the antenna PCB and the aluminum shell that combine to form the main part of the sensor, replaceable attachments were designed to fit on the underside of the sensor. The attachments can have different radii allowing the sensor to be installed on HV equipment of different sizes. They can also be replaced easily to allow the sensor to be used for periodic testing of different assets. The attachments have foam feet covered with conducting fabric which ensure that the sensor shell is electrically connected to the tank/enclosure of the equipment under test at ground potential. This also ensures that the main detecting element of the sensor, the antenna, is shielded from external interference.

V. Testing and Comparison with Simulation

In order to evaluate the capabilities of the DSB sensor and validate the results obtained by the simulations the sensor was tested in a laboratory environment. Two different tests were performed to examine its radiation characteristics and benchmark its performance against industry standards. Additionally, a bespoke rig was constructed to examine the PD detection capabilities of the sensor as well as compare its performance with similar, commercially available barrier sensors.

A. Measurement of Reflection Coefficient

The first test to evaluate the performance of the DSB sensor was to check the impedance mismatch loss over the intended operational frequency range. The reflection coefficient (S11 parameter), which describes how much of the electromagnetic energy received by the sensor is reflected, was measured using a Keysight M9370A PXIe Vector Network Analyzer (VNA) attached to a National Instruments PXIe-1073 chassis. The VNA, with a bandwidth of 0.3 – 4.0 GHz, was connected to the sensor using a 50 cm long, low-loss, semi-rigid coaxial cable rated for frequencies up to 6 GHz. The test was

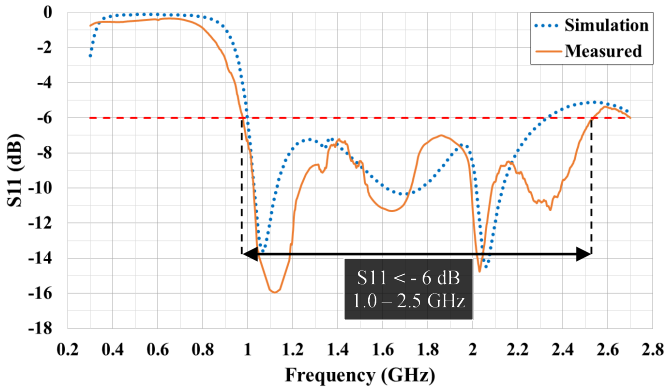

Fig. 9. Simulated and measured reflection coefficient of the Dual-Slot Barrier sensor. With a reflection coefficient of less than -6 dB, the sensor exhibits good impedance match in the frequency range of 1.0 – 2.5 GHz.

conducted under ambient conditions (temperature: 21°C, relative humidity: 42%). The sensor was mounted on a non-conducting support structure with the antenna facing an open field with no obstructions. The results of the test and a comparison with the simulation are shown in Fig. 9.

The barrier sensor exhibits a good impedance match with a reflection coefficient less than -6 dB in the frequency range 1.0 – 2.5 GHz. As shown in Fig. 9, the simulation was able to provide a very good prediction regarding the response of the sensor. In fact, the simulation appears to be slightly conservative with the measured response being better at the higher end of the frequency spectrum, between 2.2 – 2.5 GHz. The test result indicates that detected signals will be able to be transmitted with minimal losses when the sensor is connected to signal cables and instruments which have a 50 Ω impedance. Hence, there is no need to include additional impedance matching hardware to the measurement system which could potentially increase its cost and complexity.

B. Measurement of Effective Height

Another test frequently performed on UHF sensors for PD detection is the measurement of inverse antenna factor. Also known as effective height, H_e , [22] it can be used to provide an indication regarding the sensitivity of a sensor. The inverse antenna factor is defined as the ratio of the voltage output at the output terminal (connector) of the sensor, $V_{50\Omega}$, to the electric field incident on the antenna, E . It is expressed as follows:

$$H_e = \frac{V_{50\Omega}}{E} \tag{4}$$

Originally, National Grid defined limits for the effective height of sensors intended for use in 420 kV and 525 kV substations, listed in TGN(T) 121 [23]. The first limit requires the mean effective height to be greater than 6 mm, calculated over the intended frequency range of operation. The second limit mandates that a sensor should have an effective height greater than 2 mm for more than 80% of its operating frequency range. Although not part of an international standard, these limits have been adopted by various equipment manufacturers and utilities around the world when it comes to evaluating the performance of UHF PD sensors.

To check if the effective height for the DSB sensor lies within

This article has been accepted for publication in a future issue of this journal, but has not been fully edited. Content may change prior to final publication. Citation information: DOI 10.1109/JSEN.2019.2943625, IEEE Sensors Journal

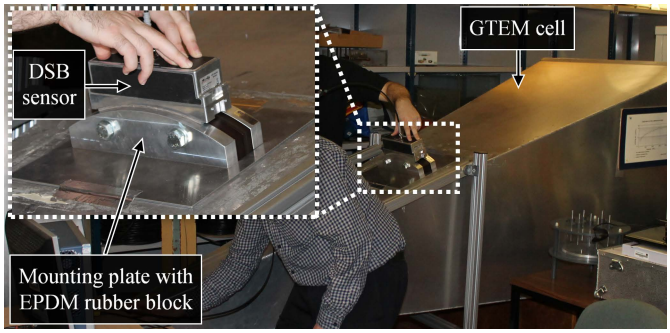

Fig. 10. Experimental test setup for measuring the Effective Height (inverse antenna factor) of the DSB sensor. The sensor is positioned on top of the GTEM cell aperture using a specially made mounting plate to emulate the installation of the sensor on gas-insulated equipment.

these limits, an FEA simulation was used as follows. The voltage at the 50 Ω coaxial lumped port used to excite the model was computed at each frequency step. This voltage was then divided by the average incident electric field computed using a probe on a boundary covering the entire front face of the sensor.

With the simulation indicating compliance with the TGN(T) 121 limits [23], measurement of the effective height was conducted with a Gigahertz Transient Electromagnetic (GTEM) cell [24]. The purpose-built GTEM cell at the University of Strathclyde [25], with which the barrier sensor was tested, was equipped with a bespoke mounting arrangement able to accommodate the sensor on its measurement aperture (Fig. 10). The arrangement, comprising an EPDM rubber block sandwiched between two metallic plates, was designed to emulate the barrier insulator used in gas-insulated equipment. The effective height measurement and a comparison with the computed values from the simulation is shown in Fig. 11.

The results of the GTEM cell measurements show very close agreement with the computed values, underlining the effectiveness of the simulation methodology in predicting the effective height performance of UHF PD sensors. Furthermore,

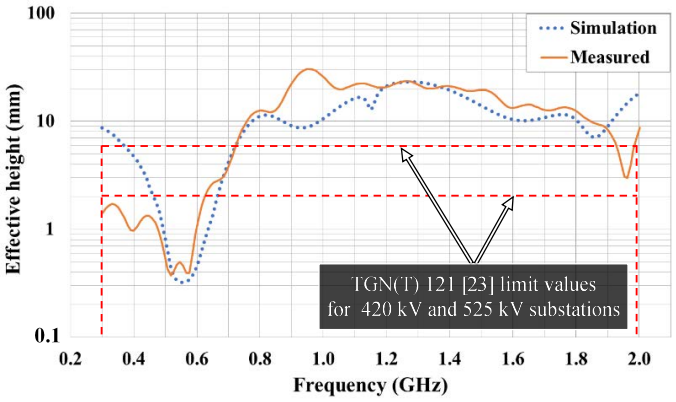

Fig. 11. DSB sensor Effective Height, H_e , (inverse antenna factor) over the 0.3 – 2 GHz frequency range showing a good match between the computed and measured results.

TABLE III
DSB SENSOR EFFECTIVE HEIGHT

	Mean effective height, H_e (mm)	Percentage effective height above 2 mm
Limits - TGN(T) 121	6.0	80%
Simulation	11.6	93%
Measured	**13.0**	**90%**

the DSB sensor exceeds the limits outlined in TGN(T) 121 by a substantial margin (Table III) in the frequency range of 0.3 – 2.0 GHz. This emphasizes the potency of the design and the ability of the sensor to be used for the condition monitoring of equipment rated up to the highest voltage.

C. *Testing the PD Detection Capabilities of the DSB Sensor*

In addition to testing the frequency response, the PD detection capabilities of the DSB sensor were also examined. A test rig, a schematic of which is shown in Fig. 12, was constructed to mimic a short section of a GIS tank with mounting points able to accommodate multiple sensors. The cylindrical tank section was positioned inside a Faraday cage during testing to minimize external interference. Because calibration of UHF PD detection systems to apparent charge is not possible, the rig can be used to test the sensitivity of UHF PD sensors by allowing implementation of the verification procedure detailed in [26] and [27].

In order to produce signals similar to those attributed to PD activity in the UHF spectrum, a pulse sharpener circuit was used to generate high-amplitude (5 – 20 V), fast-rise-time (< 5 ns) pulses. The circuit was supplied with a 5 V, 50% duty cycle square wave in order to produce pulses with a repetition rate of 10 kHz. Its output was connected to an ultra-wideband UHF planar antenna [28] via a 300 MHz high-pass filter, which was used to inject the simulated PD pulses into the test rig.

The DSB sensor can be interfaced with wide-band as well as narrow-band measurement instruments, hence both alternatives were tested. Firstly, the sensor was connected directly to a 3 GHz oscilloscope via low-loss coaxial cable. The frequency spectrum of the detected signal can be seen in Fig. 13(a) with the PD frequency content ranging between 0.8 and 1.2 GHz. The PD signal with peak amplitude just over 0.1 V is easily distinguished from background noise and other unwanted signals in the UHF spectrum. Secondly, the signal from the sensor was fed to a broadband frequency down-converter which in turn was connected to an oscilloscope. The converter was set to output a signal in the 0 - 100 MHz range which can be easily accepted by a plethora of widely available monitoring instruments. The signal after conversion from a centre

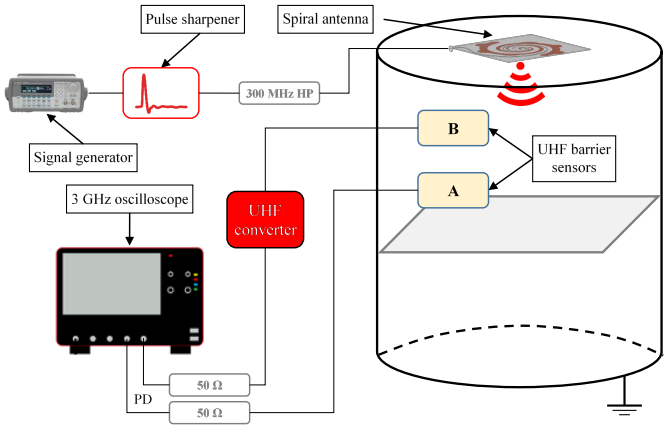

Fig. 12. Experimental test setup for testing the PD detection capabilities of UHF PD sensors and performing the sensitivity verification procedure described in [24]. The setup closely resembles a short tank section of gas-insulated equipment and has suitable attachments points for multiple internal and external sensors.

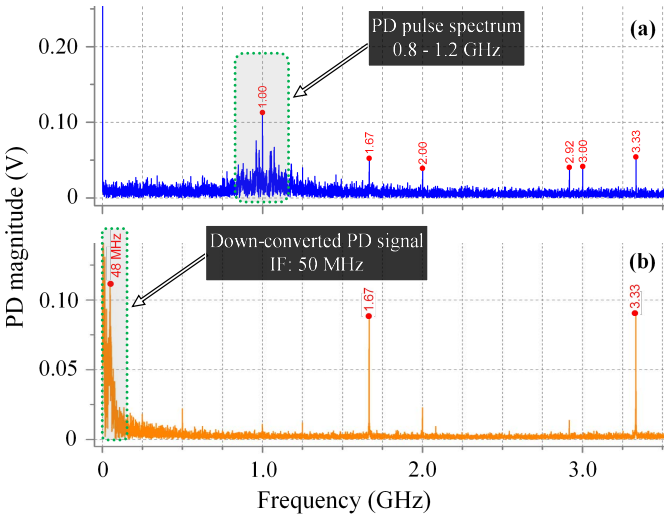

Fig. 13. Frequency spectra of the original (a) and down-converted (b) signals captured with the DSB sensor. The injected PD signal, produced with a pulse sharpener circuit, has a center frequency of 1 GHz and is down-converted from the output of the sensor to an intermediate frequency of 50 MHz.

frequency of 1 GHz to an intermediate frequency of 50 MHz is shown in Fig. 13(b).

Furthermore, the PD detection capabilities of the sensor were compared directly with those of three other commercially available sensors using the rig of Fig. 12. The sensors were attached to the rig on adjacent mounting points and a signal complying with the sensitivity verification procedure of [26] was injected into the rig. The amplitude, rise time and noise level of the detected signals from all four sensors are presented in Table IV. The DSB sensor outperforms the other three barrier sensors by a significant margin. Specifically, in terms of voltage amplitude, the DSB sensor output is 68% higher than that of Sensor 1, 179% higher than that of Sensor 2 and 231% higher than that of Sensor 3.

VI. Application to Power System Apparatus

To further evaluate the capabilities of the DSB sensor for its intended use as an external PD sensor for power system apparatus, the setup of Fig. 14 was utilized. Two DSB sensors were retrofitted onto barrier insulators of a 420 kV gas-insulated line (GIL) section located at the HV laboratory of the University of Manchester. One sensor was positioned on the

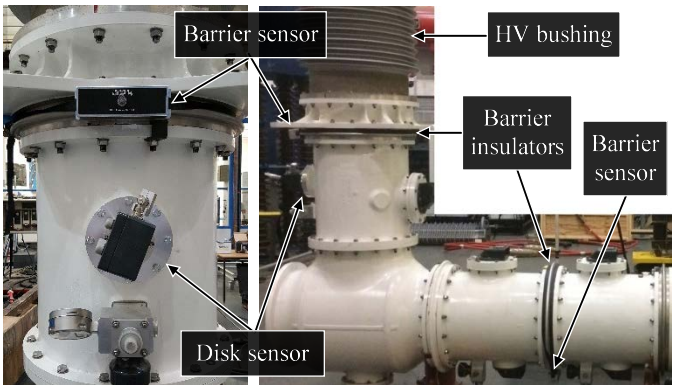

Fig. 14. Installation of two DSB sensors on top of the barrier insulator apertures of a 420 kV gas-insulated line (GIL) section. The GIL was also equipped with internal disk-type sensors.

TABLE IV
Barrier Sensor Comparison

		Amplitude (mV)	Rise time (ns)	Noise level (mV_{pk-pk})
	Injected PD signal	15.7 V	0.22	
Detected signals	Barrier Sensor 1	63	0.30	27
	Barrier Sensor 2	38	0.34	33
	Barrier Sensor 3	32	0.44	30
	DSB Sensor	**106**	**0.24**	**28**

insulator of the vertical section of the GIL, directly below the HV bushing connecting the GIL to the HV supply. The other sensor was positioned on one of the insulators separating the horizontal compartments of the GIL. The GIL was also fitted with internal disk type PD sensors before it was filled with gas.

During testing, a high amplitude, fast rise time pulse, conforming to the specifications of [26], was injected into the GIL using one of the disk sensors. The synchronized UHF signals detected by a disk sensor and the two DSB sensors, captured with a 3 GHz oscilloscope, are shown in Fig. 15. It can be observed that the amplitudes of the signals are very similar for all three sensors. Also, it is possible to distinguish the different arrival times of the UHF PD signal on each sensor. The main difference is the lower noise level of the disk sensor signal, which is to be expected since the sensor is located inside the GIL and is therefore shielded from external interference. The test results demonstrate the potency of the DSB sensor design and its suitability for effective PD detection and localization for gas-insulated power system apparatus.

VII. Conclusion

A novel barrier sensor for UHF PD detection in gas-insulated equipment has been developed and optimized using FEA simulations. Its main specifications are the following:

- Dimensions (L x W x H): 190 x 60 x 68 mm
- Bandwidth: 0.3 – 2.0 GHz (based on TGN(T) 121 [23])
- Mean effective height: 13 mm
- Effective height above 2 mm: 90%
- Output impedance: 50 Ω

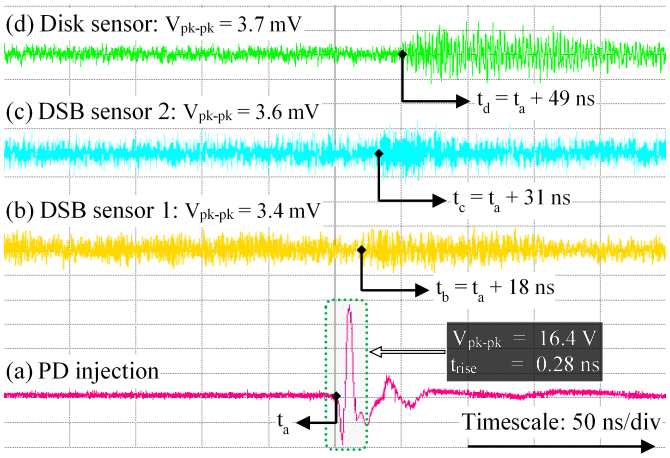

Fig. 15. UHF signals detected by an in-build disk sensor (d) and two retrofitted DSB sensors (b), (c), on a GIL section after injection of a high-amplitude, fast rise time pulse (a). Sensor signal arrival times, t_b, t_c, t_d, are shown in relation to the injected PD signal arrival time, t_a.

The unique dual-slot planar antenna, backed by an air-filled cavity, allows the sensor to overcome the constraints imposed by its restricted dimensions. As a result, the sensor exhibits wide bandwidth and good sensitivity making it ideal for detecting low-amplitude, pulsed PD signals. Comparative tests have shown that the DSB sensor outperforms similar sensors by as much as 231% in terms of signal detection amplitude. The 50 Ω output impedance, courtesy of the feeding method employed for the antenna, ensures wide compatibility with both wideband and narrowband measurement instruments, as proven experimentally. Finally, in addition to the carefully selected dimensions, replaceable sealing attachments open up additional options for retrofitting the sensor on a wide variety of equipment.

REFERENCES

[1] C. Zachariades, R. Shuttleworth, R. Giussani, and R. MacKinlay, "Optimization of a High-Frequency Current Transformer Sensor for Partial Discharge Detection Using Finite-Element Analysis," *IEEE Sensors Journal*, vol. 16, pp. 7526-7533, 2016.

[2] The British Standards Institution, "High-voltage test techniques - Partial discharge measurements," *BS EN 60270:2001+A1*, ed, 2016.

[3] J. S. Pearson, O. Farish, B. F. Hampton, M. D. Judd, D. Templeton, B. W. Pryor, and I. M. Welch, "Partial discharge diagnostics for gas insulated substations," *IEEE Transactions on Dielectrics and Electrical Insulation*, vol. 2, pp. 893-905, 1995.

[4] J. Fuhr, S. Markalous, S. Coenen, M. Haessig, M. Judd, A. Kraetge, M. Krueger, R. Lebreton, E. Lemke, S. Okabe, R. Schwarz, U. Sundermann, S. Tenbohlen, and P. Werle, "Partial Discharges in Transformers," *CIGRÉ*, vol. Technical Brochure 676 - WG D1.29, 2017.

[5] C. Neumann, B. Krampe, R. Feger, K. Feser, M. Knapp, A. Breuer, and V. Rees, "PD measurements on GIS of different designs by non-conventional UHF sensors," *CIGRÉ Session 2000*, vol. 15-305, pp. 1-9, 2000.

[6] W. Boeck, M. Albiez, T. Bengtsson, A. Diessner, R.Feger, K.Feser, A. Girodet, E. Gulski, B. F. Hampton, T. Hucker, M. D. Judd, W. Kultunowicz, L. Lundgaard, C. Maulat, A. H. Mufti, C. Neumann, A. Petit, R. Pietsch, P. Prieur, W. R. Rutgers, G. Schoffner, Y. Shibuya, and G. Wanninger, "PD detection system for GIS: sensitivity verification for the UHF method and the acoustic method," *Électra*, vol. 183, pp. 75-87, 1999.

[7] T. A. Milligan, *Modern Antenna Design*, 2nd ed. Hoboken, New Jersey: John Wiley & Sons, Inc., 2005.

[8] C. A. Balanis, *Antenna Theory: Analysis and Design*, 3rd ed. Hoboken, New Jersey: John Wiley & Sons, 2005.

[9] A. Hernández-Escobar, E. Abdo-Sánchez, and C. Camacho-Peñalosa, "A Broadband Cavity-Backed Slot Radiating Element in Transmission Configuration," *IEEE Transactions on Antennas and Propagation*, vol. 66, pp. 7389-7394, 2018.

[10] L. Quan and S. Zhongxiang, "Inverted microstrip-fed cavity-backed slot antennas," *IEEE Antennas and Wireless Propagation Letters*, vol. 1, pp. 98-101, 2002.

[11] G. Q. Luo, Z. F. Hu, L. X. Dong, and L. L. Sun, "Planar Slot Antenna Backed by Substrate Integrated Waveguide Cavity," *IEEE Antennas and Wireless Propagation Letters*, vol. 7, pp. 236-239, 2008.

[12] S. Mukherjee, A. Biswas, and K. V. Srivastava, "Broadband Substrate Integrated Waveguide Cavity-Backed Bow-Tie Slot Antenna," *IEEE Antennas and Wireless Propagation Letters*, vol. 13, pp. 1152-1155, 2014.

[13] U. Schichler and J. Gorablenkow, "Experience with UHF PD detection in GIS substations," *Proceedings of the 6th International Conference on Properties and Applications of Dielectric Materials (Cat. No.00CH36347)*, 2000, pp. 286-289 vol.1.

[14] S. A. Boggs, "Electromagnetic Techniques for Fault and Partial Discharge Location in Gas-Insulated Cables and Substations," *IEEE Transactions on Power Apparatus and Systems*, vol. PAS-101, pp. 1935-1941, 1982.

[15] J.-P. Berenger, "A perfectly matched layer for the absorption of electromagnetic waves," *Journal of Computational Physics*, vol. 114, pp. 185-200, 1994/10/01/ 1994.

[16] W. Frei. (2015). *Modeling of Materials in Wave Electromagnetics Problems*. Available: http://www.comsol.com/blogs/modeling-of-materials-in-wave-electromagnetics-problems/

[17] S. Marburg, "Six Boundary Elements per Wavelength: Is That Enough?," *Journal of Computational Acoustics*, vol. 10, 2002.

[18] R. Lee and A. C. Cangellaris, "A study of discretization error in the finite element approximation of wave solutions," *Antennas and Propagation, IEEE Transactions on*, vol. 40, pp. 542-549, 1992.

[19] W. Frei. (2013). *Meshing Considerations for Linear Static Problems*. Available: http://www.uk.comsol.com/blogs/meshing-considerations-linear-static-problems/

[20] S. Long, "Experimental study of the impedance of cavity-backed slot antennas," *IEEE Transactions on Antennas and Propagation*, vol. 23, pp. 1-7, 1975.

[21] The British Standards Institution, "Degrees of protection provided by enclosures (IP Code)," *BS EN 60529:1992+A2:2013*, ed: BSI Standards Limited, 2019.

[22] J. L. Volakis, R. C. Johnson, and H. Jasik, *Antenna engineering handbook*, 4th ed. ed.: McGraw-Hill, 2007.

[23] National Grid, "Capacitive couplers for UHF partial discharge monitoring," *TGN(T) 121*, ed, 1997.

[24] R. D. Leo, T. Rozzi, C. Svara, and L. Zappelli, "Rigorous analysis of the GTEM cell," *IEEE Transactions on Microwave Theory and Techniques*, vol. 39, pp. 488-500, 1991.

[25] M. D. Judd and O. Farish, "A pulsed GTEM system for UHF sensor calibration," *IEEE Transactions on Instrumentation and Measurement*, vol. 47, pp. 875-880, 1998.

[26] U. Schichler, W. Koltunowicz, D. Gautschi, A. Girodet, H.Hama, K. Juhre, J. Lopez-Roldan, S. Neuhold, C. Neumann, S. Okabe, J. Pearson, R. Pietsch, U. Riechert, and S. Tenbohlen, "UHF Partial Discharge Detection System for GIS: Application Guide for Sensitivity Verification," *CIGRÉ Electra*, vol. 286 - WG D1.25, 2016.

[27] The British Standards Institution, "High voltage test techniques - Measurement of partial discharges by electromagnetic and acoustic methods," *PD IEC/TS 62478*, ed: BSI Standards Limited, 2016.

[28] C. Zachariades, R. Shuttleworth, R. Giussani, and T. H. Loh, "A Wideband Spiral UHF Coupler with Tuning Nodules for Partial Discharge Detection," *IEEE Transactions on Power Delivery*, 2018.

Christos Zachariades was born in Athens, Greece, in 1984. He received the BEng (Hons) in electrical and electronic engineering, in 2009, the MSc in electrical power systems engineering, in 2010, and the PhD in electrical and electronic engineering, in 2014, from the University of Manchester, UK. He was previously a Senior Test and Development Engineer with HVPD Ltd, UK, and a lecturer with the University of Manchester, UK, and is now a lecturer in Electrical Energy with the University of Liverpool, UK. Dr. Zachariades is a Chartered Engineer (CEng) and a member of the Institution of Engineering and Technology (IET) as well as a member of the Cyprus Scientific and Technical Chamber (ETEK).

Roger Shuttleworth was born in the UK and completed his BSc and PhD degrees in electrical and electronic engineering at The University of Manchester, UK. He worked for a year at GEC Traction before joining the University as a lecturer in the Power Systems Research group and later the Power Conversion Research group. He has over 100 papers and patents and was Director for the Power Electronics, Machines and Drives MSc course. His main research activities are in the areas of Power Electronics, Energy Control and Conversion, and Energy Harvesting. He is now retired.

Riccardo Giussani (StM'10, M'13) was born in Legnano, Italy, in 1978. He received the EngD in electrical engineering from Politecnico di Milano, Italy, and the PhD in electrical and electronic engineering from the University of Manchester, UK, in 2015. Since 2013, he has been working at HVPD Ltd, UK. He is currently HVPD's Principal Development Engineer. Dr. Giussani is a member of the Institution of Engineering and Technology (IET), the IEEE Dielectrics and Electrical Insulation Society (DEIS) and the IEEE Industry Applications Society (IAS).